Histol Histopathol (2026) 41: 925-935

Histology and Histopathology
From Cell Biology to Tissue Engineering

ORIGINAL ARTICLE Open Access

# A clinicopathological study of eight cases presenting a biphasic structure: A distinct variant of pulmonary carcinoma

**Hongyu Wang[1]*, Qiuyao Li[1]*, Jiwei Ma[2], Kun Yang[3], Xiaoyan Lin[2], Huifeng Jiang[1], Yali Xu[2], Lin Song[2], Yu Zhang[2], Xiaoqian Liu[1], Zheng Mou[4], Wenjing Su[2]**

[1]Department of Pathology, Qilu Hospital (Qingdao), Cheeloo College of Medicine, Shandong University, Qingdao, [2]Department of Pathology, Shandong Provincial Hospital Affiliated to Shandong First Medical University, Jinan, [3]Central Laboratory, Affiliated Hospital of Qingdao University and [4]Department of Pharmacy, Qilu Hospital (Qingdao), Cheeloo College of Medicine, Shandong University, Qingdao, PR China

*These two authors contributed equally to this work

**Summary.** Biphasic structures, which are composed of outer basal cells and inner glandular cells, are frequently indicative of salivary gland-type tumors or benign lesions, such as bronchial adenoma, within the lung. However, the occurrence of a biphasic structure in lung cancer is rarely reported and can lead to significant challenges and confusion in diagnosis, particularly in biopsy specimens. In our study, we collected eight lung epithelial tumors that presented with a distinct biphasic structure component and examined their clinicopathological characteristics. Histological examination revealed that the biphasic structure component, often intermingled with conventional squamous cell carcinoma or adenocarcinoma, was defined by basal cells encircling the glandular epithelium. Immunohistochemical analysis demonstrated a distinctive peripheral p40 staining pattern in the biphasic structure component. Genetic analysis identified driver mutations in seven out of eight patients, which are typically associated with conventional pulmonary adenocarcinomas, including *EGFR* L858R, *EGFR* 19-del, *EGFR* 20-ins, and *KRAS* mutations. The presence of biphasic structure components in these cases confirms a genuine form of lung cancer, likely representing a variant of lung adenocarcinoma. This study's findings enhance the understanding of lung cancer's morphological diversity and caution against prematurely dismissing the malignancy potential of pulmonary epithelial lesions based solely on the presence of basal cells, especially with biopsy specimens.

**Key words:** Lung cancer, Biphasic structure, Basal cell, p40, Salivary gland-like

*Corresponding Author:* Wenjing Su, MD, PhD., Department of Pathology, Shandong Provincial Hospital Affiliated to Shandong First Medical University, Jinan 250021, P.R. China. e-mail: suwenjing2804@163.com

www.hh.um.es. DOI: 10.14670/HH-25-004

## Introduction

In the lungs, the presence of peripheral basal cells in lung epithelial lesions is often associated with benign conditions, such as bronchial adenomas (Chang et al., 2018) and peribronchiolar metaplasia (Chandler and Xu, 2022). Malignant lung tumors with a biphasic structure, composed of inner glandular and outer basal cells, are usually salivary gland-type tumors, such as epithelial–myoepithelial carcinoma (EMC) and adenoid cystic carcinoma (ACC) (Sagar et al., 2023). Lung cancers exhibiting this bidirectional differentiation have been reported only in a few case reports, and their underlying nature remains poorly understood (Wang et al., 2002; Bishop et al., 2012; Jhuang et al., 2014; Yamatani et al., 2014; Hsieh et al., 2015; Zhang et al., 2015).

In this study, we present a comprehensive review of eight cases of pulmonary carcinoma that stand out due to the presence of biphasic structure components (BSCs). These BSCs, comprised of outer basal cells and inner alveolar epithelium, exhibited a distinctive peripheral p40 staining pattern. By scrutinizing these cases, we endeavor to uncover the clinical and pathological characteristics of lung cancers with BSCs. This investigation holds the potential to significantly inform diagnostic practices and therapeutic strategies for lung cancer with BSCs.

## Materials and methods

### *Patients*

During diagnostic evaluations, an atypical pulmonary tumor with a prominent biphasic structure was encountered, which defied classification within standard disease categories. This prompted an in-depth departmental discussion, culminating in the confirmation of the tumor as a unique form of lung cancer. To deepen our understanding of this phenomenon, we conducted a comprehensive search of our pathology database from January 2013 to December 2022, employing the search terms "lung, bilayer," "lung, salivary gland-like," and "lung, bidirectional differentiation." We reviewed the relevant hematoxylin and eosin (H&E) and immunohistochemical slides and retrospectively analyzed the clinical histories. After meticulous exclusion of salivary gland-type tumors, benign pulmonary epithelial lesions, such as adenomas and peribronchial metaplasia, and cases with diagnostic ambiguity, we identified eight cases of lung cancer with a distinct BSC. The cohort included seven specimens from curative surgical resections and one from a lymph node needle biopsy. Follow-up data were procured through telephone interviews. This study was approved by the Ethics Committee of Shandong Provincial Hospital Affiliated to Shandong First Medical University (Ethical Approval No. SWYX2024-541).

### *Morphological examination and immunohistochemistry*

All H&E slides were independently reviewed by two experienced pathologists (LQY and SWJ). Immunohistochemical analysis was performed for thyroid transcription factor-1 (TTF-1, clone SPT24), Napsin A (clone MX015), P40 (clone ZR8), SMA (clone 1A4), epidermal growth factor receptor (EGFR, clone SP125), and P53 (clone MX008) using antibodies from Fuzhou Maixin Biotech CO., Ltd. The Benchmark XT autostainer (Ventana Medical Systems Inc., Tucson, AZ) was utilized for staining, employing a conventional streptavidin-biotin peroxidase complex method. Heat-induced epitope retrieval was applied for selected markers, with concurrent positive and negative controls for each immunohistochemical assay.

### *Amplification Refractory Mutation System Polymerase Chain Reaction (ARMS-PCR)*

Mutations in *EGFR*, *ALK*, *ROS1*, *KRAS*, *BRAF*, *NRAS*, *PIK3CA*, *RET*, and *HER2* were detected using ARMS-PCR. Total DNA was extracted from ten 5-μm sections of formalin-fixed, paraffin-embedded tissue with a tumor content exceeding 70%. The ADx-ARMS lung cancer-related gene detection kit (AmoyDx, Xiamen, China) was employed for ARMS-PCR analysis.

### *Whole Exome Sequencing (WES)*

WES was conducted on paraffin-embedded samples (Oebiotech, Shanghai, China). DNA extracted from these samples was electrophoresed to assess quality before library construction and capture using the Agilent SureSelect Human All Exon V6 kit (Agilent, CA, USA). High-throughput sequencing was performed on the Illumina HiSeq X-Ten platform (Illumina, CA, USA). Raw WES data were analyzed for single-nucleotide polymorphisms (SNPs) and insertions/deletions (indels) using the GATK4 HaplotypeCaller module. Variant sites were annotated with ANOVAR software and cross-referenced against databases including RefSeq, ExAC, ESP6500, gnomAD, SIFT, ClinVar, PolyPhen, MutationTaster, COSMIC, GWAS Catalog, and OMIM. Bioinformatics tools, such as PolyPhen-2 and SIFT, were utilized to predict the pathogenicity of identified variants.

## Results

### *Clinical characteristics*

Eight cases of lung cancer with a distinct BSC were identified from 20,536 cases of invasive lung cancer surgical specimens and biopsy specimens of metastatic lung cancer. In our institutes, the incidence rate of lung cancer with a BSC was 0.04% from January 2013 to December 2022. The demographic and clinical profiles of the eight patients are summarized in Table 1. The average age was 63.13±5.62 years, with a range of 51 to 70 years, and there was a notable female preponderance (six females to two males). A quarter of the patients (two out of eight) reported a history of smoking. Clinical presentations included cough, chest pain, dizziness, and nausea, each noted in a single patient, while the remaining four patients were asymptomatic upon physical examination. Computed tomography (CT) scans revealed that the majority of tumors were located in the right lung (five out of eight cases). In the seven cases with available imaging data, six showed close proximity to the bronchus, with three exhibiting central-type lesions (located in bronchi and lobar bronchi) encroaching on bronchial segments, lobes, and walls. The other three displayed peripheral lesions (located from the segmental bronchi to alveoli) with bronchial truncation or shadows. The mean tumor diameter, as measured from seven surgical specimens, was 2.36 ± 0.86 cm, ranging from 1.2 to 3.8 cm. The clinical staging varied, with five patients at stage I, two at stages II and III, and one at stage IV. All patients were followed up during the study period. One patient (Case 8, Stage IV) succumbed within a month post-biopsy. In contrast, the other seven patients survived with a mean follow-up duration of 16.00±9.20 months (ranging from 5 to 30 months), with one patient (Case 5) developing brain metastasis within 21 months.

### *Histological and immunohistochemical features*

Gross examination of the surgical resection specimen disclosed a tumor section that was grayish-white and grayish-black, with a medium to firm hardness and indistinct boundaries, which were not significantly different from typical pulmonary carcinomas. Microscopically, the tumor margins appeared infiltrative, with central areas showing cystically dilated airways. As detailed in Table 2, residual bronchial cartilages or bronchioles were identified within the tumors of the seven patients who underwent surgery.

Including cases with metastatic involvement of lymph nodes, the presence of a BSC was discernible in all eight instances (Fig. 1). BSC typically presented as two distinct layers, exhibiting mild to moderate architectural and cytological atypia. The cells lining the inner cavity surface predominantly formed a single layer (Fig. 1A,B,E-H), although a cribriform structure (Fig. 1C) or multilayered configurations (Fig. 1D) were also observed. The inner cavity cells predominantly exhibited a cuboidal or columnar epithelial appearance, characterized by an abundant, bichromatic cytoplasm. Nuclei varied in staining intensity from pale to deeply colored, with visible nucleoli in certain cases (Fig. 1B). Correspondingly, the outer cells typically adopted a cuboidal or spindle-shaped morphology with scant cytoplasm, and in some cases, the outer basal cells were challenging to discern in H&E-stained sections (Fig. 1B,C, arrows). The nuclei of the outer cells were often dense and darkly stained, indicative of basal cell characteristics, and in some cases, the chromatin of the basal cells displayed a relatively open chromatin pattern (Fig. 1A,H).

Immunohistochemical assessment revealed that p40 staining was distinctly localized to the periphery of BSCs, underscoring the presence of the outer basal cell layer. P40 staining showed that the outer basal cells generally formed a single layer (Fig. 2B1-B5,B7,B8), although they could occasionally be multilayered (Fig. 2B6). TTF1 staining exhibited variability in BSCs, ranging from complete absence to sporadic or diffuse positivity. In the majority of cases, the TTF-1 expression levels in the outer basal cells were comparable to those of adjacent inner glandular cells. For instance, in Cases 1, 2, and 8, both the outer and inner cell layers demonstrated diffuse, medium-intensity TTF1 expression. In contrast, Cases 3, 5, 6, and 7 showed a complete absence of TTF1 staining in both layers, while Case 4 exhibited only scattered and sparse TTF1-positive cells in both layers. Napsin A staining in BSCs varied from complete negativity (Fig. 2D3,D5-D8) to rare positivity (Fig. 2D1,D4) or diffuse positivity (Fig. 2D2), with any positive expression predominantly localized to the inner glandular cells. The myoepithelial marker SMA consistently showed negative staining in these basal cells (data not shown), indicating a lack of myoepithelial properties. The incidence of p53-positive tumor cells in the surgical specimens displayed a broad spectrum, with positivity rates spanning from 40% to less than 1% in most cases, as outlined in Table 2. Notably, the lymph node biopsy from Case 8 displayed

**Table 1.** Clinical characteristics of the eight cases.

| Case No. | Sex/Age (years) | Smoking history | Symptoms | Primary tumor location | Relationship with bronchus | Tumor Size (cm) | TNM/Stage (First visit) | Treatment | Follow up |
|---|---|---|---|---|---|---|---|---|---|
| 1 | Male/64 | Yes | Chest pain | Right lower lobe; Central-type lesions | Surrounding-bronchial tube walls | 2.0 | T1bN0M0/IA2 | PPL | Well/25m |
| 2 | Female/66 | No | None | Right upper lobe; Central-type lesions | Surrounding-bronchial tube walls | 3.0 | T1cN1M0/IIB | CPL+HMLNR, targeted therapy | Well/10m |
| 3 | Female/65 | No | None | Right lower lobe; Peripheral lesions | Bronchial truncation | 2.5 | T2N3M0/IIIB | PPL+biopsy of contralateral hilar lymph nodes, chemotherapy | Well/5m |
| 4 | Female/70 | No | None | Left upper lobe; Peripheral lesions | None | 1.2 | T1bN0M0/IA2 | PPL+HMLNR | Well/8m |
| 5 | Female/61 | Yes | Dizziness, nausea | Right upper lobe; Peripheral lesions | NA | 3.8 | T2aN0M0/IB | CPL+HMLNR, local radiotherapy of-brain metastasis, targeted therapy+chemotherapy | Brain metastasis/21m, well/30m |
| 6 | Female/51 | No | Cough | Right lower lobe; Peripheral lesions | Bronchial truncation | 1.7 | T1bN0M0/IA2 | CPL+HMLNR | Well/19m |
| 7 | Male/62 | No | None | Left upper lobe; Peripheral lesions | Bronchial shadows | 2.3 | T1cN0M0/IA3 | PPL+HMLNR | Well/15m |
| 8 | Female/66 | No | Cough | Left lower lobe; Central-type lesions | Surrounding-bronchial tube walls | - | T4N3M1/IV | Fine needle aspiration biopsy of cervical lymph node metastasis | Died/1m |

CPL, complete pulmonary lobectomy; PPL, partial pulmonary lobectomy; HMLNR, hilar and mediastinal lymph node resection; NA: not available.

widespread and intensely positive p53 staining in both the inner and outer cell layers (Fig. 2A8, upper right insertion). In Cases 2 and 7, EGFR-L858R staining showed partial positivity in both inner glandular cells and outer basal cells of BSCs (Fig. 3B,G) as well as adenocarcinoma. A comprehensive summary of the immunohistochemical staining results is presented in Table 2.

The proportion of BSCs varied across different cases. As detailed in Table 2, the range of BSC content in the eight specimens extended from 10% to 100%. Transitions between BSC and classical pulmonary adenocarcinoma or squamous cell carcinoma (SCC) were observed (Fig. 4A-D). As the tumor evolved from BSC to pulmonary adenocarcinoma, the peripheral p40-positive basal cells progressively diminished until they eventually vanished (Fig. 4B), while as the tumor evolved from BSC to SCC, the expression pattern of p40 gradually shifted to diffuse positivity (Fig. 4D). The pulmonary adenocarcinomas associated with BSCs exhibited the characteristic morphologies of typical lung adenocarcinomas, including lepidic (Fig. 4E), acinar

**Table 2.** Histopathological characteristics of the eight cases.

| Case NO | Residual bronchial cartilage | Residual bronchiole | Morphological components (percentage) | Immunohistochemical staining results | | | | | | |
|---|---|---|---|---|---|---|---|---|---|---|
| | | | | | | TTF-1 | NapsinA | P40 | EGFR | P53 |
| 1 | - | - | BSC (100%) | BSC | inner | + | + (rare) | - | - | + (40%) |
| | | | | | outer | + | - | + | - | |
| 2 | - | + | ADC (acinar, 60%), BSC (40%) | BSC | inner | + | + | - | + (partial) | + (5%) |
| | | | | | outer | + | - | + | + (partial) | |
| | | | | ADC | | + | + | + (rare) | + (partial) | |
| 3 | + | + | ADC (acinar, 60% micropapillary, 20%), BSC (10%), SCC (10%) | SCC | | - | - | + (partial) | - | + (5%) |
| | | | | BSC | inner | - | - | - | - | |
| | | | | | outer | - | - | + | - | |
| | | | | ADC | | + | + (rare) | + (rare) | - | |
| 4 | + | - | ADC (acinar, 80%; papillary, 10%), BSC (10%) | BSC | inner | + (scattered) | + (rare) | - | - | + (<1%) |
| | | | | | outer | + (scattered) | - | + | - | |
| | | | | ADC | | + | + | + (rare) | - | |
| 5 | + | - | SCC (80%), BSC (20%) | SCC | | + (scattered) | - | + | - | + (3%) |
| | | | | BSC | inner | - | - | - | - | |
| | | | | | outer | - | - | + | - | |
| 6 | - | + | BSC (85%), ADC (acinar, 15%) | BSC | inner | - | - | - | - | + (5%) |
| | | | | | outer | - | - | + | - | |
| | | | | ADC | | + (partial) | + | - | - | |
| 7 | - | + | ADC (acinar, 50%), ) BSC (30%), SCC (20% | SCC | | - | - | + (partial) | + (rare) | + (5%) |
| | | | | BSC | inner | - | - | - | + (partial) | |
| | | | | | outer | - | - | + | + (partial) | |
| | | | | ADC | | + (partial) | | - | + (partial) | |
| 8* | | | BSC: 100% | BSC | inner | + | - | - | - | + (100%) |
| | | | | | outer | + | - | + | - | |

BSC: biphasic structure component; ADC: adenocarcinoma; SCC: squamous cell carcinoma. *: biopsy specimen.

**Table 3.** The ARMS-PCR results and WES results of Cases 1 to 8.

| Case No. | ARMS-PCR | WES | | | | | |
|---|---|---|---|---|---|---|---|
| | Mutational site | Mutated gene | Transcript ID | Mutated site | Nucleic change | Amino acid change | VAF (%) |
| 1 | - | *OR11H6* | NM_001004480.1 | exon1 | c.775T>C | p.C259R | 40.74 |
| 2 | *EGFR* L858R | - | - | - | - | - | - |
| 3 | - | - | - | - | - | - | - |
| 4 | *EGFR* 19-del | - | - | - | - | - | - |
| 5 | *EGFR* 20-ins | - | - | - | - | - | - |
| 6 | *EGFR* 20-ins | - | - | - | - | - | - |
| 7 | *EGFR* L858R | - | - | - | - | - | - |
| 8 | - | *KRAS* | NM_033360.3 | exon2 | c.38 G>A | p.G13D | 26.50 |
| | | *TP53* | NM_000546.5 | exon7 | c.743 G>A | p.P248Q | 21.79 |

VAF, variant allele fraction.

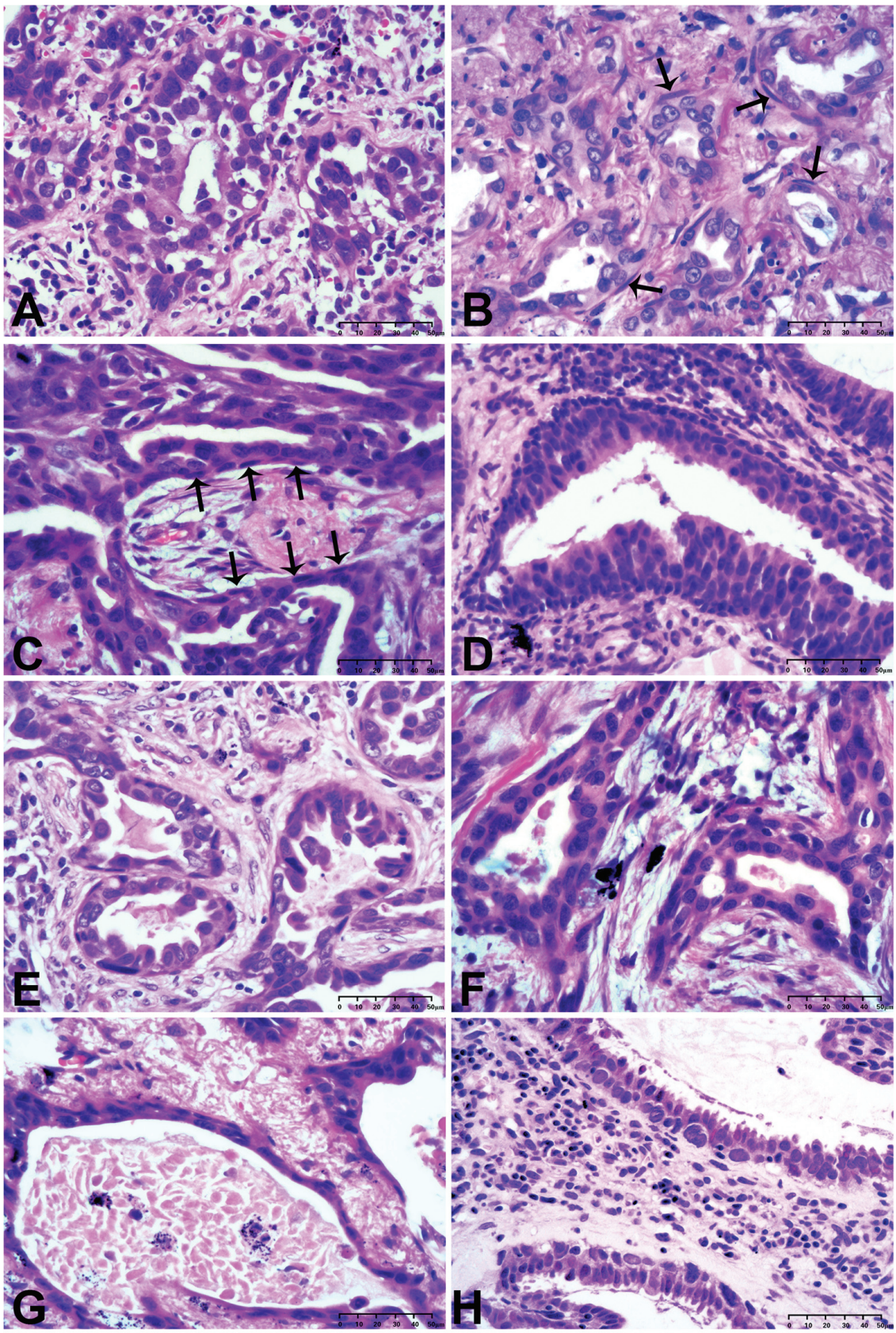


**Fig. 1.** Histological characteristics of BSCs. H&E staining revealed that the BSC in all eight cases exhibited bidirectional differentiation characteristics, consisting of an inner and an outer layer. **A-H.** sequentially display representative morphologies of BSCs from Cases 1 to 8. In most cases, the inner glandular layer is composed of simple lumens formed by a single layer of cuboidal cells. **C.** shows that in Case 3, the inner glandular cells of the BSC formed a cribriform structure, while **(D)** illustrates that in Case 4, the inner glandular epithelium was pseudostratified columnar epithelium. The outer basal cells were distinct in most cases, appearing as a single layer of spindle-shaped or cuboidal cells. However, in Cases 2 and 3, the spindle-shaped basal cells within the BSC were relatively less recognizable, as indicated by the arrows in **(B)** and **(C)**.

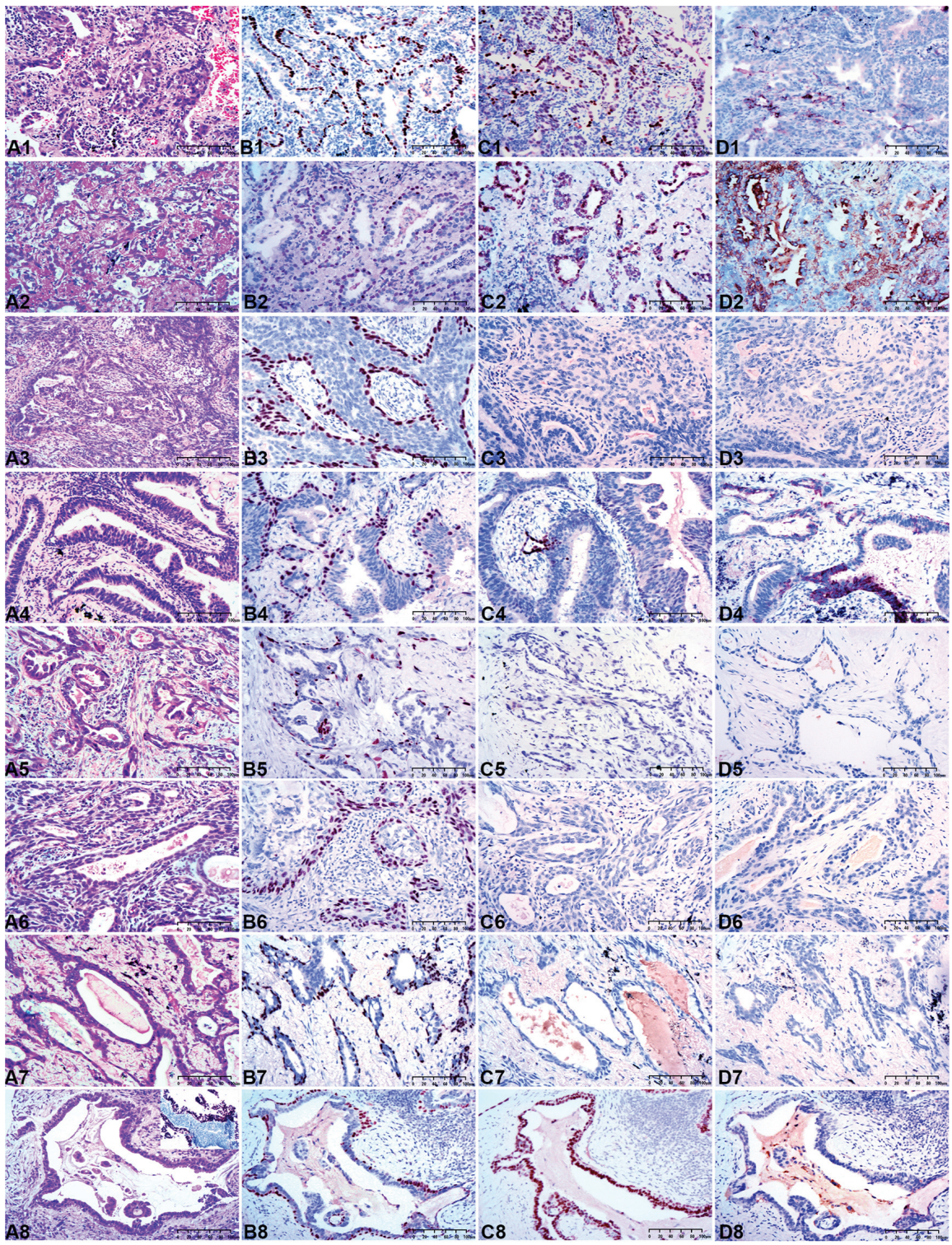


**Fig. 2.** Immunohistochemical characteristics of BSCs. The eight cases are sequentially displayed (the numbers following the letters in the images indicate the case numbers). **A1-A8** show the H&E staining morphology of the eight cases. p40-positive cells were arranged along the peripheral side of the tumor cell nests **(B1-B8)**. In most cases, the outer basal cells of BSC are single-layered, while in some cases, the basal cells can also be multilayered **(B6)**. TTF1 expression in the BSC can be completely absent, partially positive, or diffusely positive, and within the same case, the positivity rate and intensity of TTF1 in both the inner and outer layers of cells are consistent **(C1-C8)**. Napsin A expression in the BSC can be completely absent, focally positive, or diffusely positive, and its expression is mainly limited to the inner glandular epithelium **(D1-D8)**. In Case 8, both the inner and outer layer cells of the BSC showed diffuse, strong positive expression of p53 (**A8**, upper right insertion).

(Fig. 4F), papillary (Fig. 4G), micropapillary (Fig. 4H), and other complex glandular patterns, such as poorly differentiated adenocarcinomas with desmoplastic stroma (Fig. 4I), and even mucinous adenocarcinomas (Fig. 4J). Concurrent SCCs were predominantly moderately differentiated invasive SCC (Fig. 4K), and in some instances, *in situ* SCCs were also identified (Fig. 4L).

### *Molecular genetic features*

The classic targeted mutation genes *EGFR*, *ALK*, *ROS1*, *KRAS*, *BRAF*, *NRAS*, *PIK3CA*, *RET*, and *HER2* were detected in all eight patients using ARMS-PCR. As shown in Table 3, five of the eight patients harbored EGFR mutations, including two with L858R mutations in exon 21, two with insertions in exon 20, and one with deletions in exon 19.

Among the three patients with no detected mutation, two underwent further WES testing. When predicting the pathogenicity of mutation sites, mutations in the *KRAS* (Tier I) and *TP53* genes (Tier II) were found in one patient (Case 8), and the other had a mutation in the *OR11H6* gene (Tier I). These three mutations were all missense. The detailed results are shown in Table 3.

## Discussion

In the lungs, lesions with basal cells typically suggest two scenarios: salivary gland-type tumors and benign pulmonary epithelial lesions, such as pulmonary adenomas. It is generally believed that basal cells do not appear in non-salivary gland-type pulmonary epithelial malignant tumors, namely lung cancers. However, in this study, we reviewed eight pulmonary carcinoma cases containing varying proportions of BSCs, which comprised outer basal cells and inner glandular epithelium, and exhibited a characteristic peripheral p40 staining pattern. During the diagnostic process, the biphasic structure in all eight cases caused significant confusion among multiple pathologists, posing a considerable challenge for diagnosis. These cases indicate that the presence of basal cells should not be considered absolute evidence for ruling out lung cancer.

During the diagnostic process, we differentiated these cases from common tumors with basal cell differentiation. Initially, we considered salivary gland-type tumors, which typically exhibit bidirectional differentiation. Lung metastasis is most frequently observed in major salivary gland cancers, with high-grade mucoepidermoid carcinoma (MEC) and ACC having the highest rates (Benchetrit et al., 2022). However, in this series, metastasis from a primary salivary gland was ruled out due to the absence of prior malignancy and the presence of alveolar epithelium differentiation. Primary salivary gland-type tumors of the lungs are often closely associated with the bronchi, as seen in our cases. Yet, most true salivary gland-type tumors do not express the alveolar epithelial marker TTF1. Sporadic reports have indicated that the inner glandular cells of primary lung salivary gland-type tumors, such as EMCs and MECs, can express lung epithelial markers like TTF1 and surfactant protein A (SP-A) (Matsumoto et al., 2002; Chang et al., 2007; Muñoz et al., 2011; Xu et al., 2012). However, those cases had distinct boundaries, mild cell atypia, no evidence of metastasis, and a good prognosis. In contrast, all tumors in this study had indistinct boundaries and pronounced dysplasia, often accompanied by highly malignant components such as SCC and lung adeno-

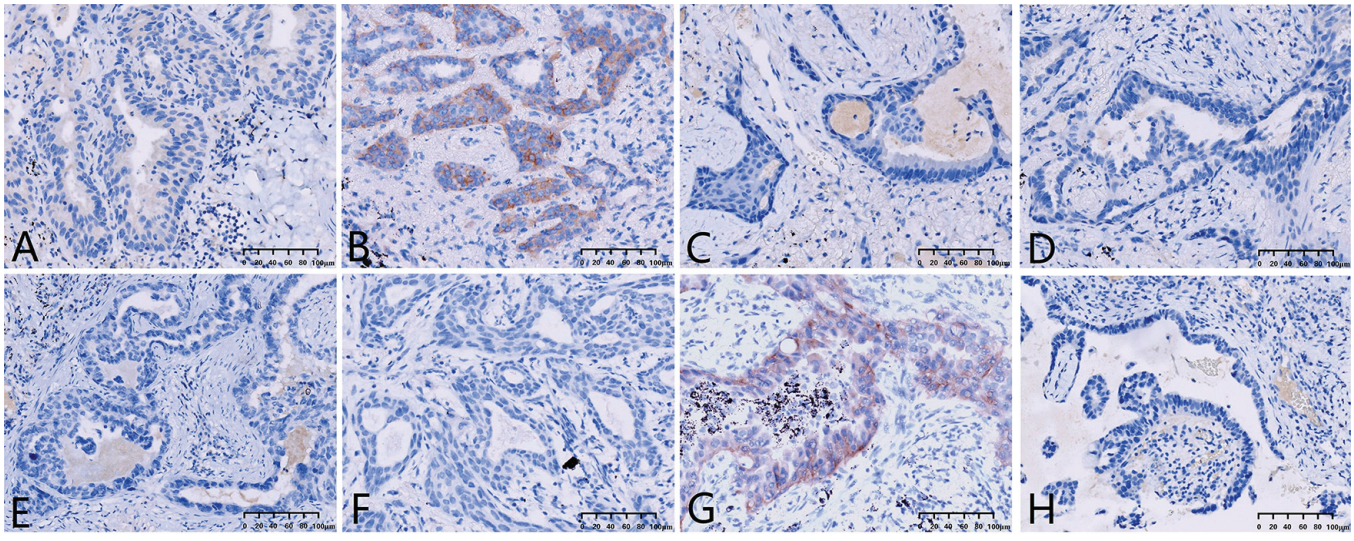


**Fig. 3.** EGFR Immunohistochemistry in Biphasic Structure components (BSC). Panels **A-H** sequentially present the EGFR-L858R staining results for Cases 1-8. Panels **B** and **G** show focal positivity in both the inner glandular and outer basal cell components of BSCs in Cases 2 and 7; the remaining six cases were entirely negative.

carcinoma. Additionally, classical gene mutations associated with lung cancer, such as *EGFR* and *KRAS*, were detected in our cases. Our cases also displayed highly malignant biological behaviors, which were starkly different from the typically low-grade malignancy of salivary gland-type cancers. Beyond these findings, detecting genes related to salivary gland tumors, including *MAML2*, *MYB*, *HRAS*, *PIK3CA*, and *AKT1*, may further aid in differential diagnosis (Urano et al., 2019; Lin et al., 2023).

In addition to true salivary gland-type tumors, it is essential to differentiate our cases from those with distal bronchiolar adenoma (BA), a benign lung lesion characterized by a bilayered bronchiolar-type epithelium with a continuous basal cell layer (Chang et al., 2018). However, BA typically presents without clinical symptoms, is small in size, well-circumscribed, lacks nuclear atypia, and rarely exhibits mitoses. In contrast, our cases predominantly exhibited pronounced clinical symptoms, extensive distribution, ill-defined boundaries, and infiltrative growth of BSCs within a desmoplastic stroma, accompanied by significant architectural and cellular atypia, which cannot be explained by BA. Although BA can undergo malignant transformation into basal cell carcinoma, mucinous adenocarcinoma, and invasive acinar adenocarcinoma (Miyai et al., 2018; Chen et al., 2021; Han et al., 2021; Wang et al., 2021), and malignant BA can have common gene mutations associated with lung adenocarcinoma, such as *KRAS* and *EGFR*, carcinomas with a biphasic structure have not been reported in the malignant transformation of BA. Therefore, the presence of BSCs in this series is also difficult to

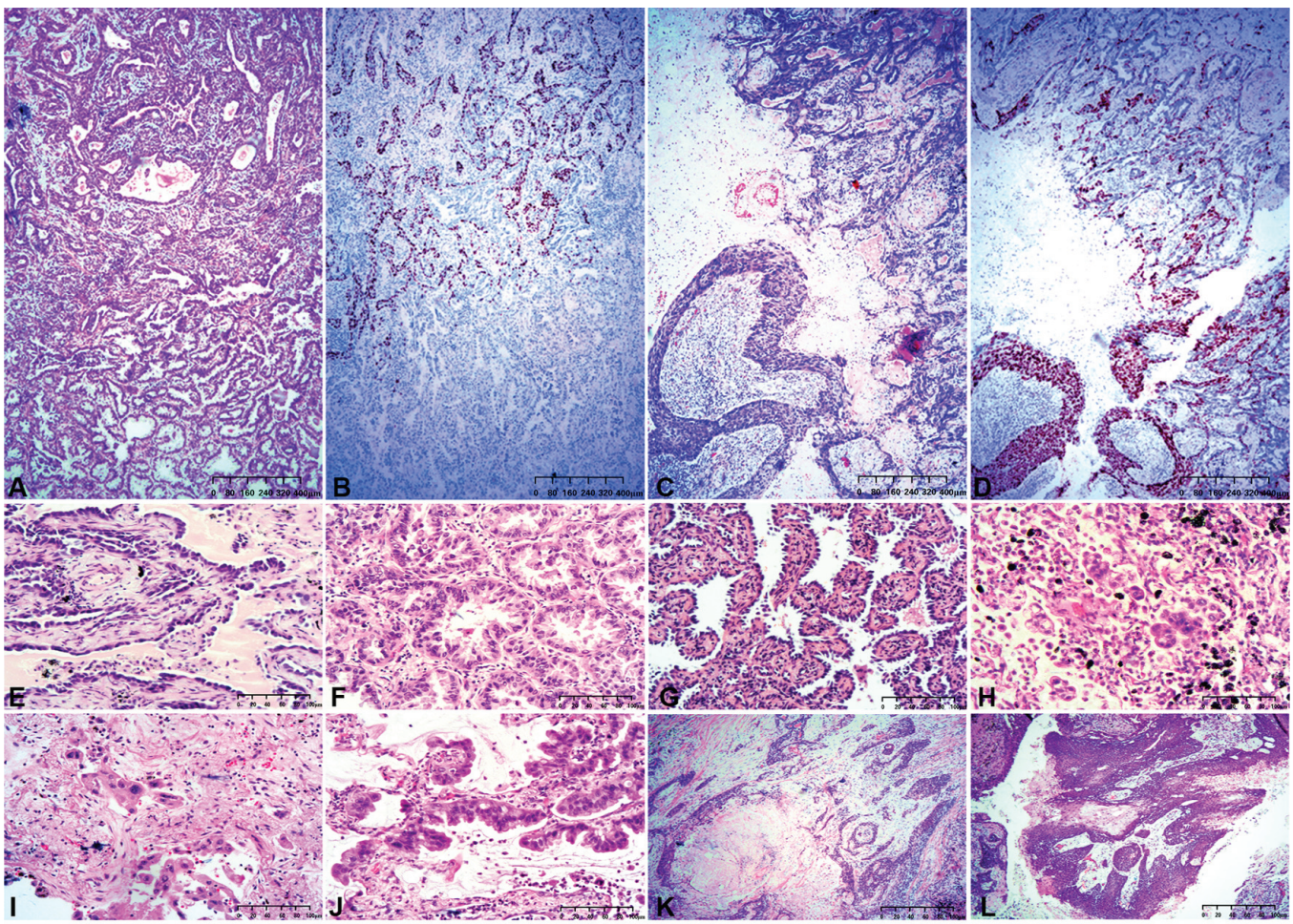


**Fig. 4.** Histological characteristics of pulmonary adenocarcinoma and squamous cell carcinoma components and their transition to BSC. BSCs occur concurrently with classical pulmonary adenocarcinoma and squamous cell carcinoma. **A** shows the transition between BSC (upper) and pulmonary adenocarcinoma (lower), while **B**, with p40 staining, illustrates the gradual disappearance of basal cells as BSC transitions to pulmonary adenocarcinoma. **C** shows the transition between BSC (upper right) and squamous cell carcinoma (lower left), and **D** demonstrates that as BSC transitions to squamous cell carcinoma, p40 staining changes from being positive only in the outer basal cells to diffuse positivity. **E-J** display the various classic morphologies of pulmonary adenocarcinoma associated with BSC, including lepidic, acinar, papillary, micropapillary, cord-like infiltration with fibrous stromal reaction, and even mucinous adenocarcinoma. **K** and **L**, respectively, show invasive squamous cell carcinoma and *in situ* squamous cell carcinoma associated with BSCs.

explain by the malignant transformation of BA.

Another benign pulmonary lesion with a bilayered structure is peribronchiolar metaplasia. However, peribronchiolar metaplasia is typically a more widespread process involving inflammation or irritation of small airways, affecting many of them, and should not result in discrete nodules detectable by radiology. Grossly, peribronchiolar metaplasia does not present as an identifiable lesion. Microscopically, peribronchiolar metaplasia is often associated with a background of interstitial lung disease or inflammatory processes, and its cells consist of normal respiratory epithelium, which lacks atypia (Chandler and Xu, 2022). This is in stark contrast to the more extensive and well-defined space-occupying lesions formed by BSCs in our cases.

After excluding classic salivary gland tumors, distal BA, and peribronchial metaplasia, it seems that the only plausible explanation for this group of cases is lung cancer accompanied by BSCs. In fact, the clinical, radiological, histological, and genetic testing of these cases also support their malignant nature. However, we considered another possibility: that only the classic SCC and adenocarcinomas in this group are truly malignant components, while the BSC is formed by the extension of adenocarcinoma into pre-existing airways, with the outer basal cells not being true neoplastic elements. Yet, first, the widespread and complex nature of BSC lesions, exhibiting an irregular infiltrative growth pattern with desmoplastic stromal reaction, cannot be explained by the usual "cancer involving airways" observable only under the microscope and the orderly arrangement of airway tracts; second, in some cases, despite thorough sampling, only the BSC pattern was identified, with no possibility of classic pulmonary adenocarcinoma involving the airways; third, in the sole lymph node biopsy sample, only the BSC structure was present, and since there were no airways within the lymph node, it cannot be explained by cancer involving the airways. Finally, as immunohistochemical staining can provide a more precise cellular localization, we performed EGFR (clone SP125, which can specifically detect L858R mutations in exon 21) and p53 immunohistochemical staining in all cases, in search of evidence supporting the neoplastic nature of the outer basal cells. In accordance with the ARMS-PCR results, in Cases 2 and 7, both the outer and inner layers of the BSC exhibited positive EGFR staining, which indicated that both layers were genuine neoplastic components. In addition, in Case 8, both layers of the BSC showed diffuse and strong positive expression of p53, indicating that both the outer basal cells and the inner glandular epithelium had concurrent missense mutations in *TP53* (this result was later confirmed by WES). This supports that outer basal cells, like the accompanying inner glandular epithelium, are neoplastic components. Based on these reasons, we believe that the outer basal cells of BSCs, like the inner luminal epithelium, are indeed true malignant components.

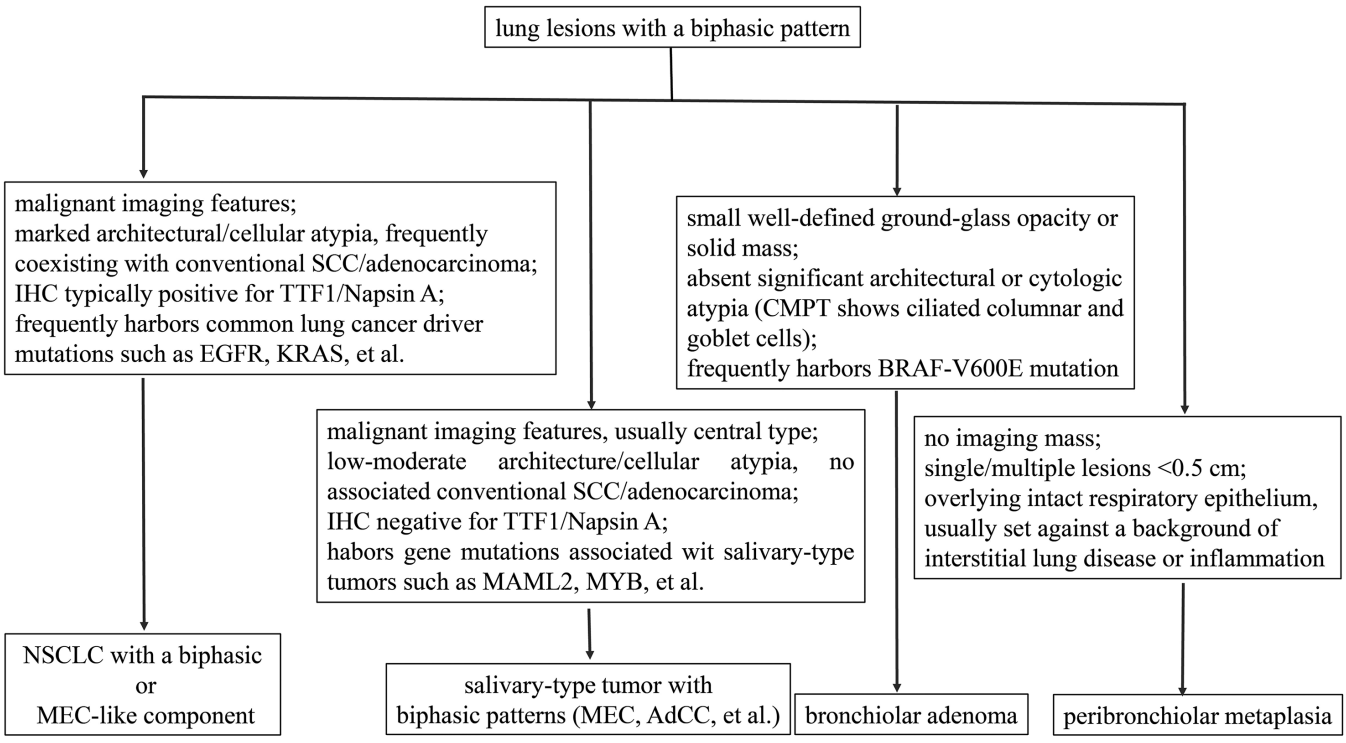


**Fig. 5.** A diagnostic algorithm for differentiating lung tumors with biphasic patterns.

In fact, lung cancers with a BSC structure and a peripheral p40 staining pattern may not be unprecedented in the literature. A literature review has shown that in two cases of lung adenosquamous carcinoma, a unique basaloid p63-staining pattern was observed in focal gland-like structures. Another report mentioned three cases of lung adenocarcinoma with a peculiar 'basal-like' staining pattern of p40 and p63, but neither were explored in depth (Wang et al., 2002; Bishop et al., 2012). Yamatani reported distinctive pulmonary adenosquamous carcinomas with a MEC-like component, characterized by a surrounding P63-positive staining pattern. In this series, all eight patients had tumors with mixed adenocarcinomatous, squamous cell carcinomatous, and MEC-like components in variable proportions, but without *MAML2* gene rearrangement (Yamatani et al., 2014). In another three pulmonary carcinomas with an MEC-like component, characteristic driver mutations of conventional lung adenocarcinomas, such as those in *EGFR* and *ALK*, were detected (Jhuang et al., 2014; Hsieh et al., 2015). Zhang et al. also described a series of pulmonary carcinomas with an MEC-like component. Despite the morphological similarities to classic salivary gland carcinomas, the authors argue that these should be classified as lung adenocarcinomas with MEC-like structures due to their highly malignant biological behavior, which is more akin to adenosquamous carcinomas (Zhang et al., 2015). Similar to the previously reported cases, the BSC in our series was mostly accompanied by varying proportions of SCC and lung adenocarcinoma, and the characteristic driver mutations of conventional lung adenocarcinomas, such as *EGFR* and *KRAS*, could be detected in nearly all patients. We speculate that these patients, akin to the aforementioned lung cancers with MEC-like components, essentially harbor highly malignant lung carcinomas rather than the typically low-grade salivary gland-type tumors. The diagnostic algorithm shown in Figure 5 may help differentiate lung tumors with biphasic structure patterns. We postulate that lung cancers with BSCs might originate from multipotent stem cells in the bronchial epithelium, and the BSC may mimic the morphology of the canals of Lambert, which represent epithelium-lined tubular communications between bronchioles and alveoli.

In conclusion, our study presents a series of lung carcinomas characterized by a distinctive BSC and a peripheral p40-staining pattern, posing a significant challenge in diagnostic discernment, particularly in biopsy specimens. The underlying nature of these pulmonary carcinomas with BSCs suggests classification as adenosquamous carcinomas, which are highly malignant entities that require differentiation from genuine salivary gland-type tumors and benign pulmonary conditions, such as BA and peribronchiolar metaplasia. Although its morphology differs from that of classic adenosquamous carcinoma, this rare mixed-type lung cancer also harbors the common driver mutations characteristic of lung adenocarcinoma, and patients with advanced-stage disease may benefit from targeted therapy. This investigation not only broadens the pathologists' grasp of the morphological spectrum of lung cancer but also underscores that the mere presence of basal cell layers should not be construed as definitive evidence to rule out high-grade malignant neoplasms. A precise diagnosis in such cases can be achieved through a holistic integration of clinical presentations, radiological characteristics, histological configurations, and genetic testing outcomes.

*Acknowledgements.* This work was supported by grants from the Natural Science Foundation of Shandong Province (grant numbers ZR2022LSW001, ZR2021QH306, ZR2023QH031, ZR2021QH199) and Qingdao Outstanding Health Professional Development Fund.

*Conflict of interest statement.* The authors declared that they have no conflicts of interest.

*Author contributions.* Roles/Writing - original draft: Wang Hongyu; Investigation: Li Qiuyao; Methodology: Ma Jiwei, Yang Kun, Lin, Xiaoyan, and Mou Zheng; Data curation: Jiang Huifeng, Xu Yali, Song Lin, Zhang Yu, and Liu Xiaoqian; Roles/Writing - review & editing: Su Wenjing.

*Ethics approval statement.* This study was approved by the Ethics Committee of Shandong Provincial Hospital Affiliated to Shandong First Medical University (NO. SWYX2024-541).

## References

Benchetrit L., Mehra S., Mahajan A., Rahmati R.W., Judson B.L. and Edwards H.A. (2022). Major salivary gland cancer with distant metastasis upon presentation: Patterns, outcomes, and imaging implications. Otolaryngol. Head Neck Surg. 167, 305-315.

Bishop J.A., Teruya-Feldstein J., Westra W.H., Pelosi G., Travis W.D. and Rekhtman N. (2012). p40 (ΔNp63) is superior to p63 for the diagnosis of pulmonary squamous cell carcinoma. Mod. Pathol. 25, 405-415.

Chandler C.M. and Xu H.D. (2022). Atypical adenomatous hyperplasia *versus* peribronchiolar metaplasia. In: Practical lung pathology. Springer International Publishing. pp 21-25.

Chang T., Husain A.N., Colby T., Taxy J.B., Welch W.R., Cheung O.Y., Early A., Travis J.W. and Krausz T. (2007). Pneumocytic adenomyoepithelioma: a distinctive lung tumor with epithelial, myoepithelial, and pneumocytic differentiation. Am. J. Surg. Pathol. 31, 562-568.

Chang J.C., Montecalvo J., Borsu L., Lu S.H., Larsen B.T., Wallace W.D., Sae-Ow W., Mackinnon A.C., Kim H.R., Bowman A., Sauter J.L., Arcila M.E., Ladanyi M., Travis W.D. and Rekhtman N. (2018). Bronchiolar adenoma: Expansion of the concept of ciliated muconodular papillary tumors with proposal for revised terminology Based on morphologic, immunophenotypic, and genomic analysis of 25 cases. Am. J. Surg. Pathol. 42, 1010-1026.

Chen F., Ren F., Zhao H., Xu X.Q. and Chen J. (2021). Mucinous adenocarcinoma caused by cancerization from a ciliated multinodular papilloma tumor: A case report. Thorac. Cancer 12, 1629-1633.

Han X., Hao J., Ding S., Wang E.H. and Wang L. (2021). Bronchiolar adenoma transforming to invasive mucinous adenocarcinoma: A case report. Onco Targets Ther. 14, 2241-2246.

Hsieh M.S., Lee Y.H., Chen J.S., Lee J.M. and Chang Y.L. (2015). Mixed mucoepidermoid carcinoma and adenocarcinoma of the lung: Two cases with unusual histologic features. Lung Cancer 89, 80-83.

Jhuang J.Y., Chou Y.H., Hua S.F. and Hsieh M.S. (2014). Mixed lung mucoepidermoid carcinoma and adenocarcinoma with identical mutations in an epidermal growth factor receptor gene. Ann. Thorac. Surg. 98, 695-697.

Lin J.L., Wu C.Y., Hou L.K., Huang Y., Xie H.K., Wu W. and Zhang L.P. (2023). Clinicopathological and molecular genetic features of primary pulmonary epithelial-myoepithelial carcinoma. Zhonghua Bing Li Xue Za Zhi. 52, 715-717.

Matsumoto M., Sonobe H., Furihata M., Nonami Y., Ohmori Y. and Ohtsuki Y. (2002). A case of salivary gland-type mixed tumor of the lung differentiating toward type II alveolar epithelial cells in glandular components with a literature review. Virchows Arch. 441, 618-621.

Miyai K., Takeo H., Nakayama T., Obara K., Aida S., Sato K. and Matsukuma S. (2018). Invasive form of ciliated muconodular papillary tumor of the lung: A case report and review of the literature. Pathol. Int. 68, 530-535.

Muñoz G., Felipo F., Marquina I. and Agua C.D. (2011). Epithelial-myoepithelial tumour of the lung: A case report referring to its molecular histogenesis. Diagn. Pathol. 6, 71.

Sagar A.E., Salhab M., Shah A., Strange C.D., Ahuja J., Shrof G.S., Sablof B.S., Groot P.M., Truong M.T., Cesar A. and Moran C.A. (2023). Salivary gland-type tumors of the lung. Thorax. 411-449.

Urano M., Nakaguro M., Yamamoto Y., Hirai H., Tanigawa M., Saigusa N., Shimizu A., Tsukahara K., Tada Y., Sakurai K., Isomura M., Okumura Y., Yamaguchi H., Matsubayashi J. and Nagao T. (2019). Diagnostic significance of HRAS mutations in epithelial-myoepithelial carcinomas exhibiting a broad histopathologic spectrum. Am. J. Surg. Pathol. 43, 984-994.

Wang B.Y., Gil J., Kaufman D., Gan L., Kohtz D.S. and Burstein D.E. (2002). P63 in pulmonary epithelium, pulmonary squamous neoplasms, and other pulmonary tumors. Hum. Pathol. 33, 921-926.

Wang F., Shen M.H., Cao D. and Lv J.H. (2021). Malignant ciliated muconodular papillary tumors of the lung: A case report. Int. J. Surg. Pathol. 29, 520-552.

Xu H.T., Lin X.Y., Li Q.C. and Wang E.H. (2012). The alveolar epithelial differentiation of glandular inner lining cells in a mucoepidermoid carcinoma of the lung: A case report. Diagn. Pathol. 7, 137.

Yamatani C., Abe M., Shimoji M., Maniwa T., Takahashi S., Isaka M., Ohde Y., Watanabe R., Ito I., Kondo H. and Nakajima T. (2014). Pulmonary adenosquamous carcinoma with mucoepidermoid carcinoma-like component with characteristic p63 staining pattern: Either a novel subtype originating from bronchial epithelium or variant mucoepidermoid carcinoma. Lung Cancer. 84, 45-50.

Zhang B., Lin J. and Da J. (2015). Diagnosis value of TTF-1, Napsin A and Ki-67 index in primary salivary gland-type lung carcinomas. Zhonghua Bing Li Xue Za Zhi. 44, 499-503.

Accepted October 15, 2025